

Bond behavior of reinforcement in Lightweight Aggregate Self-Compacting Concrete



Michael I. Kaffetzakis*, Catherine G. Papanicolaou

Civil Engineering Department, University of Patras, Patras, Greece

HIGHLIGHTS

- Pumice sand replacement with normal-weight one considerably increases bond strength.
- All-LWASCC bond strength (splitting) is by approx. 80% lower than that of NWSCC.
- All-LWASCC bond strength (pull-out) is by max. 30% lower than that of NWSCC.
- Bond length increase leads to decreasing of the max. normalized bond stress, τ_u^* .
- Increase of bar dia. increases/decreases τ_u^* for pull-out/beam tests, respectively.

ARTICLE INFO

Article history:

Received 6 October 2015
Received in revised form 1 March 2016
Accepted 17 March 2016

Keywords:

Lightweight self-compacting concrete
Bond strength
Pumice

ABSTRACT

An investigation of the steel-to-concrete bond in Lightweight Aggregate Self-Compacting Concrete (LWASCC, comprising exclusively pumice aggregates) is presented based on direct pull-out and beam tests. Experimental parameters include: rebar diameter, bond length and type of additive used in the LWASCC mixture. The results are compared with those obtained from identical specimens made of: (i) pumice aggregate self-compacting concrete (PASCC) with normal-weight sand and (ii) normal-weight SCC (NWSCC). The majority of specimens exhibited failures due to splitting (at relatively low slips) and rebar pull-out for direct pull-out and beam tests, respectively. Empirical formulations are used to predict experimentally derived bond strengths.

© 2016 Elsevier Ltd. All rights reserved.

1. Introduction

1.1. Lightweight Aggregate Self-Compacting Concrete (LWASCC)

The term Lightweight Aggregate Self-Compacting Concrete (LWASCC – also known as Self Compacting Lightweight Concrete, SCLC) refers to a high performance material that combines benefits stemming from Lightweight Aggregate Concrete (LWAC), such as improved durability and reduced dead loads [1–3], diminished formwork pressure (when compared to normal-weight concrete [4]), and resistance against fire [5] and chemical attack [6] with the flowability and cohesiveness of Self-Compacting Concrete (SCC).

The obvious conflict between low density and self-compactness (which in turn depends on the dynamic energy of the mixture; hence, its density) as well as that between the tendency for

lightweight aggregate (LWA) buoyancy and cohesiveness, necessitates the need for a rigorous mix proportioning for LWASCC.

In the past decade numerous studies have been conducted on LWASCC mainly consisting of artificial LWAs (expanded shale, expanded clay etc.). These results indicate that the production of structural LWASCC is feasible for a variety of air-dry densities (ranging from 1350 kg/m³ to 2000 kg/m³) and compressive strengths (ranging from 15 MPa to 60 MPa) with a retention of self-compacting capacity up to 2 h [7,8] and excellent durability characteristics [9–11].

The use of natural lightweight aggregates, such as pumice, in LWASCC reduces the production cost but also calls for a more complex mix design procedure due to the higher water absorption capacity and to the lower strength of these aggregates. Only a few studies have been conducted on LWASCC comprising natural aggregates. Uygunoğlu and Topçu [12], produced LWASCC containing pumice aggregates and investigated the effect of the aggregate type on the coefficient of thermal expansion by comparing NWSCC and PASCC mixtures. The produced mixtures exhibited sufficient self-compactness with PASCC having higher coefficient of thermal

* Corresponding author.

E-mail addresses: mkaffetzakis@upatras.gr (M.I. Kaffetzakis), kpapanic@upatras.gr (C.G. Papanicolaou).

expansion but rather low compressive strength (15–24 MPa). Papanicolaou and Kaffetzakis [13] also produced all-lightweight structural PASC having adequate flowability, moderate strength (30 MPa) and low dry density (1400 kg/m^3). A comprehensive state-of-the-art on LWASCC is given in [14].

1.2. Steel-to-concrete bond behavior

Steel-to concrete bond can be characterized as one of the most important mechanisms in reinforced concrete (RC) structures subjected to bending and shear. As Gambarova [15] highlights, bond is directly connected to: i) the achievement of the ultimate tensile and compressive strength in RC members, ii) the limitation of cracking, iii) secure development of the desirable ductility, iv) member stiffening after first cracking through tension stiffening and v) enforcing concrete toughness in the case of fiber-reinforced concrete.

Three mechanisms contribute to the build-up of bond strength:

- 1) steel-to-concrete adhesion which is owed not only to the interlocking between cement paste particles and surface micro-undulations of the steel rebar, but also to a potential chemical interaction between the aforementioned components [16];
- 2) friction between the surfaces of steel and that of the hardened surrounding concrete; and
- 3) for deformed reinforcing bars, steel-to-concrete mechanical interlock.

The latter two mechanisms are activated after the failure of adhesion as the applied load increases.

1.3. Steel-to-NWSCC and steel-to-LWASCC bond behavior

Lack of information regarding bond characteristics of pumice aggregate concrete is one of the main barriers to its acceptance in the construction industry [17]. Furthermore, no studies on steel-LWASCC bond strength have been tracked by the authors, except the work done by Lachemi et al. [18], Karahan et al. [19] and Wu et al. [20]. On the contrary, steel-SCC bond is receiving increasing attention by the research community [21–26] in an effort to experimentally evaluate the effect of SCC's fresh-state qualities on the interaction and force transfer between the solidified matrix and the steel reinforcement.

The main drive for SCC development was the elimination of structural deficiencies related to poor mechanical compaction such as weak steel–concrete bond. Therefore, theoretically, in the case of normal-weight SCC, the improved rheological features lead to improved filling ability, enhanced rebar–concrete interface quality and better steel–concrete bond conditions [27]. Additionally, the comparative study of phenomena such as the top bar effect (the effect of air and/or water entrapment underneath the top layer of horizontally placed steel bars on their bond) in vibrated concrete (VC) and SCC (both normal-weight) has received considerable attention by the academia. Based on the existing experimental data it could be postulated that the top-bar effect in SCC is – conditionally – smaller than in VC [conditions mainly referring to: a rational base of comparison between SCC and VC (that is, a set of comparable characteristics that are crucial for the phenomenon, such as bleeding potential, segregation tendency and surface settlement) and a well-designed SCC of the high static stability]. For a detailed and in-depth analysis of the pertinent state-of-the-art see the work of Khayat and Desnerck [28].

In general, the bond strength of LWAC (derived from pull-out tests) is always lower than that of normal-weight concrete of the same tensile strength showing a 15% reduction for rebar diameters

of 12, 16 and 20 mm (CUR Report 173 [29]). When pumice aggregates are used in vibrated concrete [17,30] the normalized bond strength of deformed bars (being the bond strength divided by the square root of the concrete compressive strength) is found to be by 5%–15% lower than that of normal-weight concrete, provided that the same failure mode occurs. This percentage decreases with increasing rebar embedment length and concrete age.

Lachemi et al. [18] compared NWSCC and LWASCC with different types of artificial lightweight aggregates. The findings of the study proved expanded shale aggregates to produce LWASCC with higher pull-out strength when compared to mixes containing lightweight slag aggregates. Compared to NWSCC the bond strength was reduced by 16% and 38%, for expanded shale and slag aggregates, respectively.

Karahan et al. [19] investigated the influence of metakaolin addition in LWASCC on the rheological and mechanical properties of the produced mixes. The steel-to-LWASCC bond strength was determined using direct pull-out cylinder specimens. A mean value for the bond strength of the produced specimens was approximately 3.5 MPa. Results indicated a 12% bond strength gain for a 15% metakaolin addition (by cement weight).

More recently, in 2013, Wu et al. [20] conducted a comprehensive study on steel-to-LWASCC bond behavior, investigating the bar diameter, rebar cover, LWASCC compressive strength and lateral pressure effect on the bond strength of cubic specimens. The researchers concluded that the rebar cover and the lateral pressure values affect the failure mode of the specimens, while a critical rebar cover value for splitting failure was found to be $4.5 \times \varnothing$.

This work aims to contribute to the knowledge regarding steel-to-lightweight self-compacting concrete bond focusing on the use of natural pumice aggregates.

2. Experimental program

2.1. Concrete materials and proportions

Constituent materials for PASC and control NWSCC mixes comprised natural pumice aggregates of mean particle density equal to 1200 kg/m^3 [fractions: sand 0–4 mm, fine 4–8 mm and coarse 8–16 mm], normal-weight river sand, Portland fly ash – pozzolan cement [CEM II/B-M(P-W-L) 42.5N], limestone filler (LF), silica fume (SF), polycarboxylic ether polymer superplasticizer and stabilizer. The sieve analysis of all powder materials and aggregates is given in Fig. 1. Pumice aggregates were used in a saturated condition during mixing.

The mixes were produced according to the Optimum Packing Point (OPP) concept [31]. All-pumice aggregate SCC mixes with the designation LF comprised exclusively limestone additives while mixes with the designation SF comprised both limestone and silica fume additives. Pumice sand was fully replaced by normal-weight sand in mixes LF_{NS} and SF_{NS}. Finally, in mixes LF_{NW} and SF_{NW} all pumice aggregate fractions were replaced by normal-weight calcareous ones of the same size. Table 1 summarizes the mix proportions and the oven-dry densities for all produced mixes. The fresh-state test results of the mixes are shown in Table 2 along with the 28-day compressive strength derived from triplets of $150 \times 150 \times 150 \text{ mm}$ moist-cured cube specimens.

2.2. Test specimens and configurations

For the scope of this study 72 pull-out specimens and 32 beam specimens were produced aiming to investigate the influence of: (i) SCC type (all-lightweight, lightweight with normal-weight sand or else 'sanded' and normal-weight), (ii) rebar diameter ($\varnothing = 12 \text{ mm}$ & $\varnothing = 16 \text{ mm}$) and (iii) bond length (50 & 100) on the steel-PASC bond characteristics. In direct pull-out tests all six different mixes were investigated whereas in beam tests mixes with pumice aggregates and normal-weight sand were excluded. For each individual combination of parameters three identical pull-out specimens and two identical beam specimens were constructed and tested.

Specimens regardless of type are assigned the notation X_YZ, X standing for the mix designation (as in Table 1), Y is the rebar diameter in mm and Z is the bond length expressed as a multiple of the rebar diameter used. For example, specimens LF₁₂.5 (both of pull-out and beam type) comprise mix LF with a 12 mm diameter rebar and a 60 mm (50) bond length.

During the preliminary phase of the experimental program it was shown that when tested most pull-out specimens with longer bond lengths (namely, specimens comprising groups LF_{NS}12.10, LF_{NW}12.10, LF_{NW}16.10, SF_{NS}12.10,

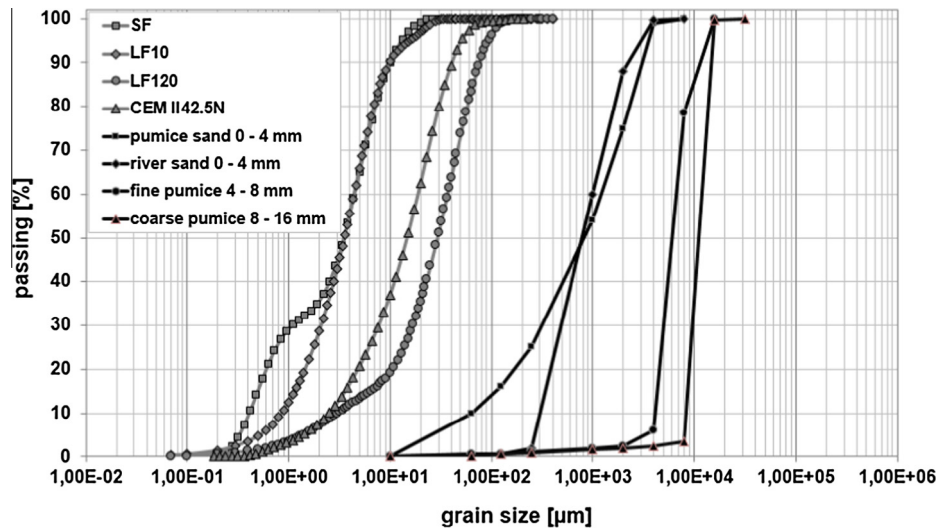


Fig. 1. Sieve analysis of all powder materials and aggregates.

Table 1

Mix designs and oven-dry densities for all SCC mixes.

Materials	Proportions [kg/m ³]					
	LF	SF	LF_NS	SF_NS	LF_NW	SF_NW
Cement	425.0	379.0	425.0	379.0	425.0	379.0
Limestone filler	149.0	94.0	149.0	94.0	149.0	94.0
Silica fume	–	30.5	–	30.5	–	30.5
Pumice Sand ^a	398.5	344.5	–	–	–	–
River Sand ^a	–	–	732.0	700.0	732.0	700.0
Fine pumice ^a	92.5	120.5	92.5	120.5	–	–
Coarse pumice ^a	205.5	268.0	205.5	268.0	–	–
Fine NWA ^a	–	–	–	–	519.0	290.0
Coarse NWA ^a	–	–	–	–	223.0	676.5
Superplasticizer	6.4	5.7	6.4	5.7	6.4	5.7
Stabilizer	2.1	1.9	2.1	1.9	2.1	1.9
Efficient water ^b	183	151	182.5	151.0	183.0	151.0
Oven-dry density	1595	1483	1766	1635	2172	2141

^a All aggregates regarded in air-dry condition; indicative values for water absorption potential are 25.0% and 3.0% for pumice and normal-weight aggregates (NWA), respectively.

^b Efficient water = moisture in aggregates + water added + admixture water – water absorbed by aggregates.

Table 2

Fresh- & hardened-state test results for all SCC mixes.

Mix	Air [%]	Slump-flow [mm]	V-funnel [s]	L-box [H ₂ /H ₁]	28-Day compressive strength [MPa]
LF	2.75	850	7.1	1.00	33.2
SF	3.50 ^a	575	3.0	0.82	34.5
LF_NS	2.25	880 ^b	5.6	1.00	38.2
SF_NS	5.25 ^a	610	3.9	0.85	37.7
LF_NW	1.50	725	6.0	1.00	45.8
SF_NW	2.00 ^a	650	3.5	1.00	46.1

^a Relatively high air contents were related to SF addition.

^b Non-conforming value as per EN 206 [32]; nevertheless, no segregation was observed.

SF_NS_16_10, SF_NW_12_10 and SF_NW_16_10) and beam specimens of groups LF_NW_12_5 and SF_NW_12_5 resulted invariably in steel yielding before any splitting or pull-out phenomena occurred; therefore, these specimen groups are not presented herein and the respective test results (plus any other related to steel yielding) are excluded from the data processing and analysis that follows. In total, 51 pull-out specimens and 26 beam specimens are exploited.

Direct pull-out specimen geometry followed partly the recommendations given in Rilem-FIP-CEB [33] differences being the type of specimens employed (cylinders, in this work), the additional bond length tested (10 times the bar diameter, in this work) and the length of the projecting part of the bar to the point of application of the tension force (200 mm, in this work). The bars extended beyond the two sides of

the specimens; bars were unbonded for a length equal to their bond length starting from the face of the specimen from which the longer part of the bar protruded. The unbonded length was achieved by using plastic sleeves around the rebars (tubes of marginally larger diameter), sealed at both ends with plasticine in order to avoid mortar penetration. Specimen dimensioning is given in Fig. 2.

Beam specimens were designed according to EN10080 – Annex C [34]. Further to the provisions of this standard regarding bond length an additional bond length was tested (5 times the bar diameter). The beams consisted of two distinct steel-reinforced concrete parts connected with a metal hinge at the top. A single rebar went through the two concrete parts, extruding approximately 200 mm from each side. Each concrete part comprised a single bonded length for the rebar. The geom-

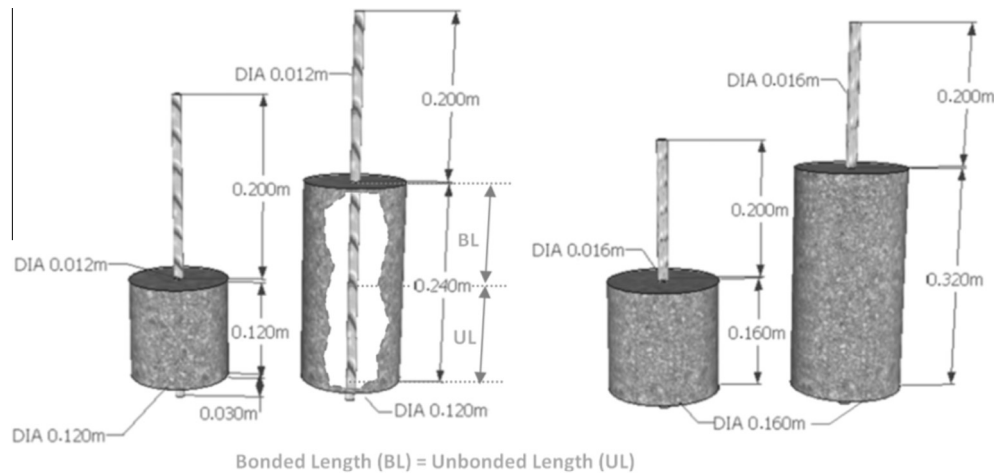


Fig. 2. Dimensions of direct pull-out specimens.

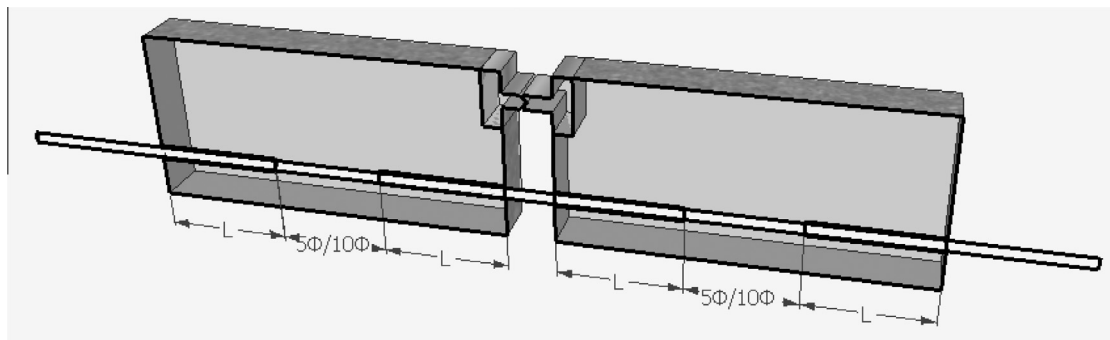


Fig. 3. Geometry of beam-type specimens.

Table 3
Beam specimens' dimensions.

Beam type	Rebar diameter [mm]	Bonded length [mm]	Unbonded length L [mm]	Cross-section dimensions	
				Height [mm]	Width [mm]
X_12_5	12	60	63.8	180	100
X_12_10	12	120	127.5	180	100
X_16_5	16	80	110.0	240	150
X_16_10	16	160	220.0	240	150

etry of the beam specimens is given in Fig. 3; the dimensions differentiate for different rebar diameter and bond length. The exact dimensions for each specimen are given in Table 3. The reinforcement details are given in Fig. 4a and b for beam specimens X_12_10 and X_16_10, respectively.

B500C steel grade deformed bars were used with a yield stress of 563 MPa, a tensile strength of 684 MPa and an ultimate strain equal to 11.5% [values determined from axial testing of six coupon specimens (three per diameter) representative of the batch of bars used for the tests]. Mean values of the nominal cross section, rib height, distance between ribs and relative rib area for each rebar diameter used in this work are given in Table 4; rib pattern illustrations are also included.

Direct pull-out tests were conducted using a universal testing machine. Specimens were placed in a custom-made supporting device comprising a stiff steel frame, as shown in Fig. 5a. In order to ensure self-alignment of the testing rig with the loading axis the former was suspended from the fixed part of the testing machine through a hinged connection. The end of the longer part of the protruding bar was fixed to the moving head of the testing machine (a 250 kN actuator) by hydraulic means. Tests were performed in a displacement-controlled mode at a rate of 0.012 mm/s and 0.016 mm/s for Ø12 and Ø16 bars, respectively. Slip between the steel bar and the concrete cylinder was measured using an extensometer. Each test was run in a fully computerized manner and was completed when either one of the following situations occurred: (i) sharp load reduction following a splitting failure

of the concrete cylinder and (ii) considerable load reduction following a rebar pull-out failure. Data from all instrumentation devices were automatically recorded using a programmable data acquisition system.

Beam specimens were subjected to four-point bending (Fig. 5b). All specimens except for X_16_10 were tested using the same testing machine used for direct pull-out tests. Specimens X_16_10 were tested using a stiff steel frame (Fig. 5c); in this case, the loading protocol was applied using a vertically positioned 500 kN actuator. The load application points were 50 mm and 70 mm distant from the inner face of the beams for X_12 and X_16 specimens, respectively. The distance between the outer face of the beams and the support points was equal to 30 mm and 70 mm for X_12 and X_16 specimens, respectively. The piston's displacement application rates were identical to the ones used during the direct pull-out tests. Conclusion of the testing procedure occurred when either a pull-out failure accompanied by a significant load reduction, or steel yielding was evidenced. Relative concrete-to-rebar displacements were measured by two LVDTs placed on the opposite sides of the in issue rebar.

2.3. Direct pull-out test results and discussion

In the case of direct pull-out tests, bond stresses are calculated according to Eq. (1).

$$\tau_i = \frac{P_i}{\pi \cdot \Phi \cdot \ell_b} \quad (1)$$

where τ_i (in MPa) and P_i (in N) are the shear stress and respective load at characteristic points of the shear stress – slip curve (i.e. at slippages $i = 0.01, 0.1$ and 1.0 and at maximum load where $i = u$), Φ is the rebar diameter in mm and ℓ_b (in mm) is the bonded length of the rebar.

Direct pull-out test results are given in Table 5 in terms of: (i) bond strength (bond stress corresponding to the maximum load recorded during the test, τ_u), (ii) normalized bond strength (bond strength divided by the square root of 28-day compressive strength, $\tau_u/\sqrt{f_c}$), (iii) ultimate slip (at the moment when splitting failure occurs, s_u), (iv) bond stress at slippage of 0.01 mm, 0.1 mm, 1.0 mm and their mean value ($\tau_{0.01}$, $\tau_{0.1}$, $\tau_{1.0}$ and τ_m , respectively) and (v) failure mode (splitting or pull-out). Tabulated values correspond to mean values calculated from a triplet of specimens for each specimen group and to the standard deviations thereof (values

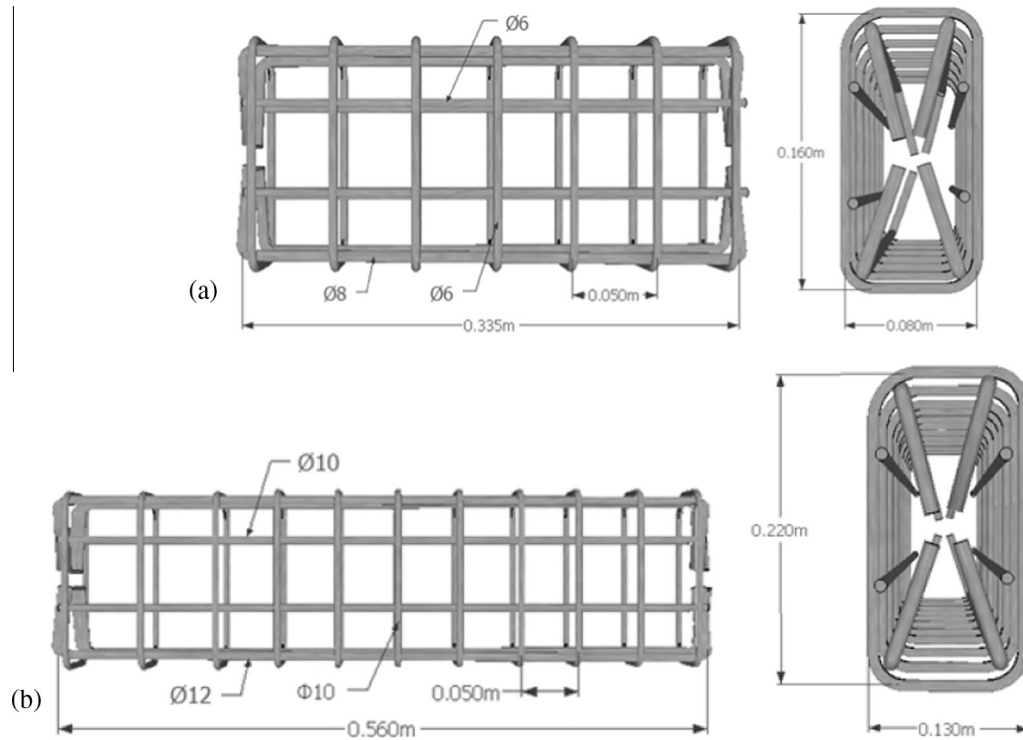




Fig. 4. Reinforcement details for beam specimen: (a) X_{12_10} and (b) X_{16_10}.

Table 4
Rebar geometry.

Rebar diameter [mm]	Nominal cross section [mm ²]	Rib height [mm]	Rib distance [mm]	Relative rib area ^a [–]	Rib pattern
Ø12	113.0	1.01	7.20	0.0438	
Ø16	201.0	1.32	9.60	0.0420	

^a The projection of all ribs on a plane perpendicular to the longitudinal axis of the steel reinforcement bar divided by the rib spacing and the nominal circumference.

in parentheses). Bond stresses $\tau_{0.01}$, $\tau_{0.1}$, $\tau_{1.0}$ and τ_m [with $\tau_m = (\tau_{0.01} + \tau_{0.1} + \tau_{1.0})/3$] – although not required by Rilem-FIP-CEB [33] – are provided for the sake of comparison with respective values derived from beam tests (as required by EN10080 – Annex C [34]).

Comparisons are more meaningful between specimen groups sharing the same basic mix design [i.e. specimens (LF...)_Y_Z from one hand and (SF...)_Y_Z from the other, as (LF...) mixes differed from the (SF...) ones in both water-to-cementitious materials ratio and aggregates-to-mortar volumetric ratio]. Nevertheless, comparisons between specimen groups cast with concrete of different mix designs may be attempted on the basis of comparable specific strengths achieved (i.e. compressive strength divided by oven-dry density, here varying between 0.021 and 0.023 MPa \times kg⁻¹ \times m³).

In Fig. 6 representative bond stress – slip curves are presented for all specimen groups. Fig. 7 illustrates typical splitting failures representative for the majority of the tested specimens. Visual inspection of failed specimens (focusing on the rebar imprint on the concrete) revealed macro defect-free rebar encapsulation. It is mentioned that casting direction was parallel to the rebars.

In general, increase of both bond length and bar diameter (where applicable) led to decreasing of the maximum normalized bond stress as shown in Fig. 8. This is attributed to the fact that the probability of occurrence of an imperfection critical for damage initiation increases as the rebar-concrete interface becomes larger. Doubling the bond length resulted in maximum normalized bond stress decrease in the range of 15%–25% (except for LF₁₆ and SF₁₂ groups for which τ_u remained unaffected). The respective decrease for increasing bar diameter (by 33%) ranges between 5% and 20% (except for the SF_{Y_5} group for which τ_u was slightly increased when dia. 16 mm bars were used in place of dia. 12 mm ones).

The replacement of lightweight (pumice) sand by a normal-weight river one leads to considerable increases in both the bond strength (absolute and normalized) and the ultimate slip value. More specifically, maximum normalized bond strength increased by approximately 40% for specimens made of pumice aggregate self-compacting concrete comprising limestone fillers. For specimens cast with mixes containing silica fume (and limestone fillers) the respective increase ranged between 60% and 120%. It is noted that these mixes (SF) were characterized by higher aggregates-to-mortar volumetric ratio compared to the LF mixes and, hence, the influence of sand replacement was expected to be more pronounced.

At rib scale, bond stress and slip are determined by the material properties of the mortar and the (fine) aggregates, the rib pattern of the rebar, the load transfer between mortar and aggregates and the rate of energy dissipation through fracture and crushing of mortar and aggregates [35]. Fig. 9a shows the rebar imprint on a split half-specimen cast with all-lightweight SCC (LF_{12_5}); both sheared-off mortar wedges and intact (smooth) mortar menisci can be identified. Additional energy dissipation mechanisms develop in matrices containing normal-weight aggregates (as – for example – in the sanded lightweight SCC, used in this work). As shown in Fig. 9b [rebar imprint on a split half-specimen cast with sanded lightweight SCC (LF_{NS_12_5})], normal-weight sand particles act as crack deviators resulting in the shearing-off of a larger portion of inter-rib mortar (in respect to the all-lightweight SCC case) both lengthwise and depthwise. According to [36], at the initial stage of the specimens' response (i.e. at low levels of bond loads) slip is the result of mortar crushing in front of the ribs; with increasing slip the detached mortar wedges move along with the rebar forming effective rib fronts that eventually – at increased levels of slip and through wedging action – cause splitting of the surrounding concrete. Based on the preceding discussion and by inspecting Fig. 9 (and

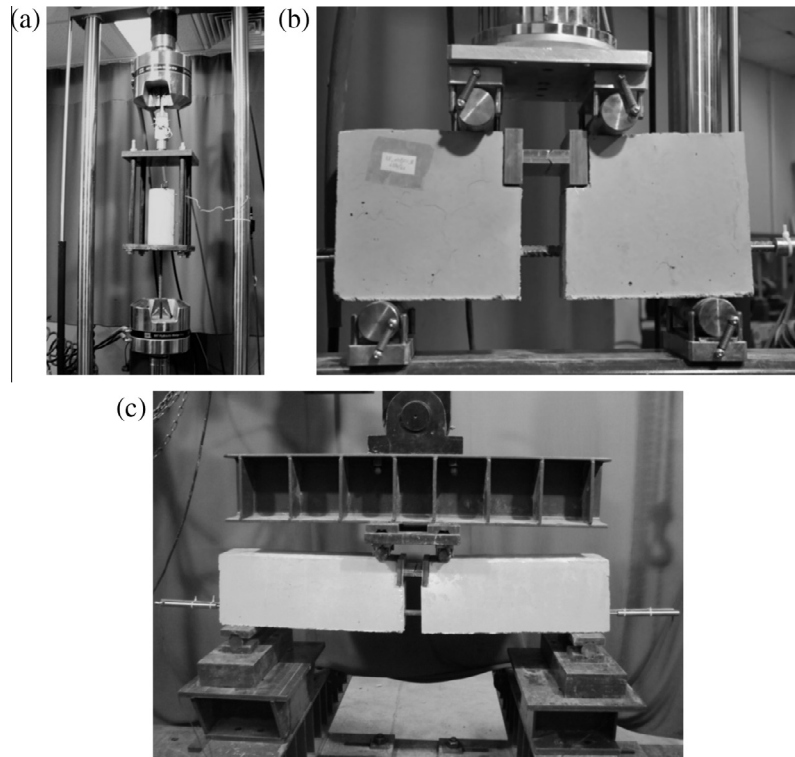


Fig. 5. Test set-ups: (a) for direct pull-out; (b) for beam tests (all beam specimens except X_16_10); and (c) for beam tests (for X_16_10 beam specimens).

Table 5
Direct pull-out test results.

Specimens	Bond strength	Normalized bond strength	Ultimate slip					Failure mode
	τ_u [MPa] (St. dev.)	τ_u^* [MPa] ^{1/2} (St. dev.)	s_u [mm] (St. dev.)	$\tau_{0.01}$ [MPa] (St. dev.)	$\tau_{0.1}$ [MPa] (St. dev.)	$\tau_{1.0}$ [MPa] (St. dev.)	τ_m [MPa] (St. dev.)	S/P ^a
LF_12_5	15.47 (2.13)	2.62 (0.36)	0.23 (0.08)	5.28 (1.57)	13.97 (0.38)	– ^b	– ^b	S
LF_12_10	13.00 (0.36)	2.20 (0.06)	0.09 (<0.01)	9.55 (1.48)	– ^b	– ^b	– ^b	S
LF_16_5	13.17 (0.75)	2.23 (0.13)	0.20 (<0.01)	5.50 (0.85)	12.47 (0.83)	– ^b	– ^b	S
LF_16_10	12.11 (0.59)	2.05 (0.10)	0.26 (0.03)	8.32 (0.35)	11.36 (0.51)	– ^b	– ^b	S
LF_NS_12_5	22.46 (0.85)	3.63 (0.14)	0.62 (0.07)	2.88 (0.12)	13.65 (0.60)	– ^b	– ^b	S
LF_NS_16_5	18.42 (0.25)	2.98 (0.04)	1.12 (0.09)	1.17 (0.22)	7.67 (0.80)	18.23 (0.13)	9.02 (0.36)	S
LF_NS_16_10	13.43 (0.48)	2.17 (0.08)	0.94 (0.28)	1.18 (0.39)	6.66 (0.94)	13.66 (0.24)	7.36 (0.33)	S
LF_NW_12_5	26.49 (0.76)	3.88 (0.11)	1.96 (0.05)	7.47 (2.60)	10.58 (2.12)	26.30 (0.45)	11.09 (0.25)	2S/1P
LF_NW_16_5	21.16 (0.39)	3.10 (0.06)	1.66 (0.06)	1.46 (0.10)	11.95 (0.22)	20.99 (0.37)	8.60 (0.55)	S
SF_12_5	9.88 (1.17)	1.67 (0.17)	0.33 (0.06)	0.99 (0.18)	7.98 (0.28)	– ^b	– ^b	S
SF_12_10	10.07 (2.67)	1.68 (0.45)	0.27 (0.10)	0.77 (0.03)	7.11 (0.36)	– ^b	– ^b	S
SF_16_5	11.11 (1.69)	1.85 (0.28)	0.42 (0.11)	1.16 (0.38)	7.07 (0.65)	– ^b	– ^b	S
SF_16_10	9.61 (1.45)	1.60 (0.24)	0.28 (0.05)	1.61 (0.16)	7.76 (1.03)	– ^b	– ^b	S
SF_NS_12_5	22.68 (2.30)	3.69 (0.37)	0.56 (0.04)	0.83 (0.04)	7.94 (0.40)	– ^b	– ^b	S
SF_NS_16_5	18.11 (1.33)	2.95 (0.22)	0.73 (0.30)	1.09 (0.06)	10.07 (0.46)	– ^b	– ^b	S
SF_NW_12_5	21.30 (0.33)	3.19 (0.05)	1.19 (0.06)	0.32 (0.01)	3.23 (0.09)	21.11 (0.31)	6.17 (0.33)	P
SF_NW_16_5	19.83 (0.13)	2.97 (0.02)	1.66 (0.09)	0.36 (0.01)	3.62 (0.23)	18.91 (0.20)	5.73 (0.28)	2S/1P

^a S for splitting failure, P for pull-out failure; for specimen groups LF_NW_12_5 & SF_NW_16_5 maximum slip value corresponds to specimens with splitting failure type.

^b Slippage values not reached.

Fig. 7) the following remarks are made: The surface boundaries of mortar wedges in the case of all-lightweight SCC are smooth as cracks propagate through the fine lightweight sand particles (with a diameter larger than the rib height, which is approximately equal to 0.08Ø, in mm). Due to the limited fracture toughness of lightweight aggregate matrices the wedging action of the effective rib fronts leads to splitting failure at low slip values. In sanded lightweight SCC, cracks follow the outer limits of the paste-aggregate interfacial zone forcing the mortar wedges to pivot about the normal-weight sand particles and disintegrate further in front of the ribs, thus, allowing for larger slips; pivoting pushes the concrete away from the bar generating circumferential tensile stresses in the concrete leading (again) to splitting failure.

Generally, the maximum normalized bond stress and the ultimate slip increase with increasing concrete density, this increase being significant in the range of 1550 kg/m³–1700 kg/m³ (in oven-dry density terms – see Fig. 10). Results from

NWSCC [37,38,23] and LWASCC [18,20] studies are also illustrated in Fig. 10. The former are associated to both pull-out and splitting failure modes, whereas the latter only to splitting ones. Strength gains for densities close to or higher than the upper oven-dry density limit for lightweight concrete (2000 kg/m³) are limited. This is owed to the secondary role that the coarse aggregates play in the bond transfer mechanism.

Strength-wise, specimens cast with all-lightweight aggregate LF mixes outperform their counterpart ones cast using SF mixes. A plausible reasoning for this behavior is given hereafter. As reported by Trezos et al. [38], silica fume addition to SCC mixes introduces higher air void contents resulting in a small reduction of τ_u . In the current study, this effect was combined with the inferior de-aeration potential characterizing all-Lightweight Aggregate Self-Compacting Concretes. The effect of silica fume addition on τ_u diminishes when partial or full pumice aggregate replacement takes place.

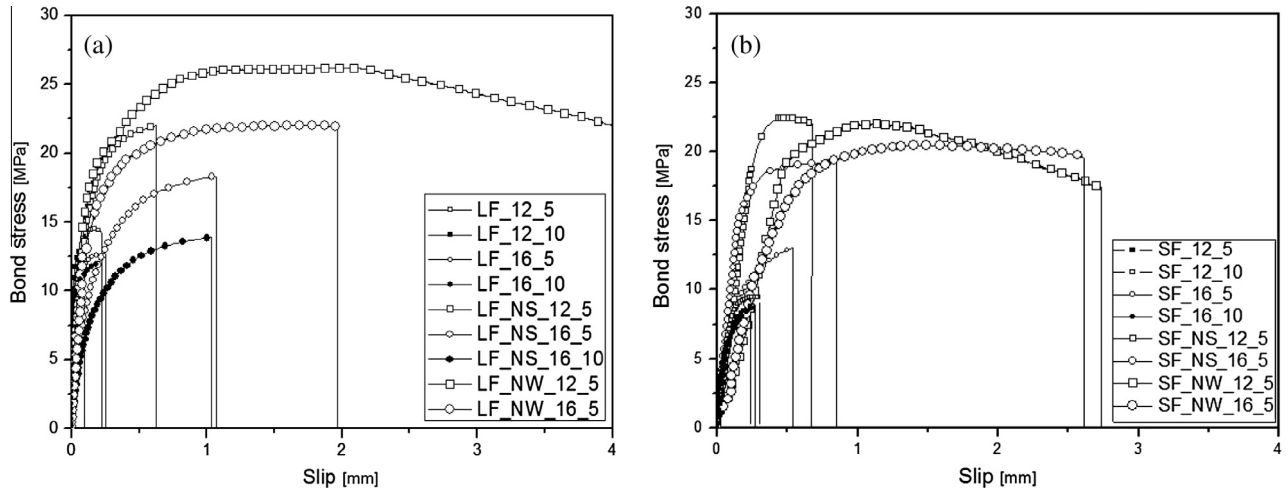


Fig. 6. Representative bond stress – slip curves for direct pull-out specimens: a) LF_Y_Z and b) SF_Y_Z.

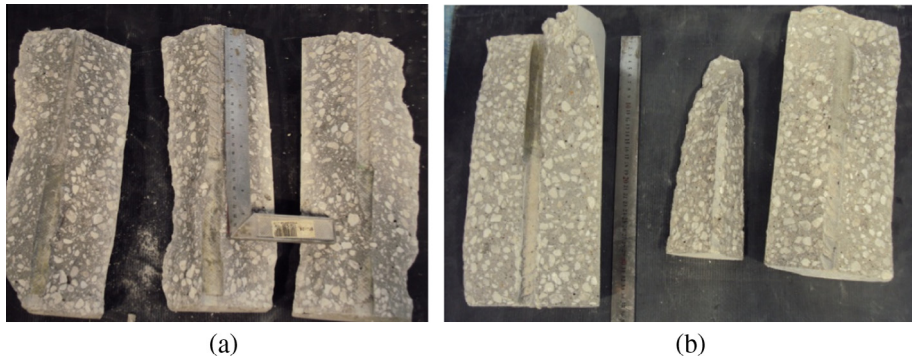


Fig. 7. Representative splitting failure: (a) LF_16_10 and (b) LF_NS_16_10.

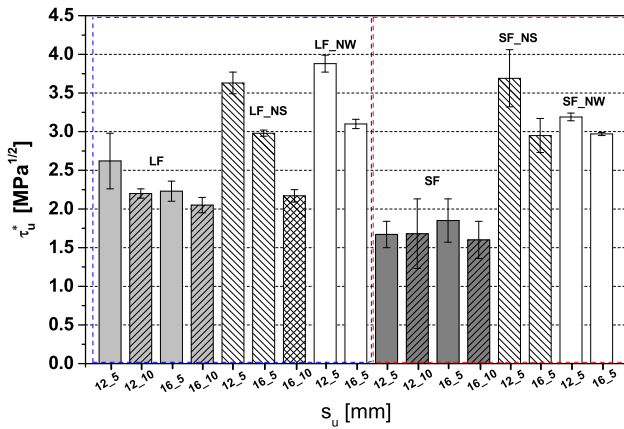


Fig. 8. Maximum normalized bond stress for direct pull-out tests.

Comparing the results of the current study with those provided by Lachemi et al. [18] (referring to LWASCC of comparable compressive strengths and higher densities) it is seen that the former correspond to higher maximum normalized bond stress values. The disadvantage of brittle splitting failure at low slip values for PASCC can be alleviated when confinement conditions are present (transverse compression or transverse reinforcement). This is evidenced by the results presented in the next section.

2.4. Beam test results and discussion

The tensile stress developed in the rebar at a given slip is given in Eq. (2).

$$\sigma_i = \frac{T_i}{A_s} = \frac{P_i L_s}{2d A_s} = \beta \frac{P_i}{A_s}, \text{ where } \beta = \frac{L_s}{2d} \quad (2)$$

where T_i and P_i are the tensile force exerted on the rebar and the total force applied to the beam at a given slip, respectively, L_s is the shear span and d is the lever arm between the hinge and the rebar. The rebar-to-concrete bond stress at a given slip, τ_i , is given in Eq. (3).

$$\tau_i = \frac{T_i}{\pi \phi \ell_b} = \frac{A_s \sigma_i}{\pi \phi \ell_b} = \frac{A_s \sigma_i}{\pi \phi (v \phi)} = \frac{\sigma_i}{4v}, \text{ where } v = \frac{\ell_b}{\phi} \quad (3)$$

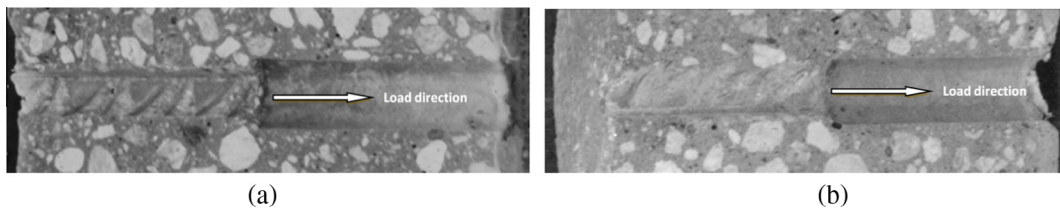


Fig. 9. Close-up of the rebar imprint on a split half-specimen cast with: (a) LF_12_5 and (b) LF_NS_12_5.

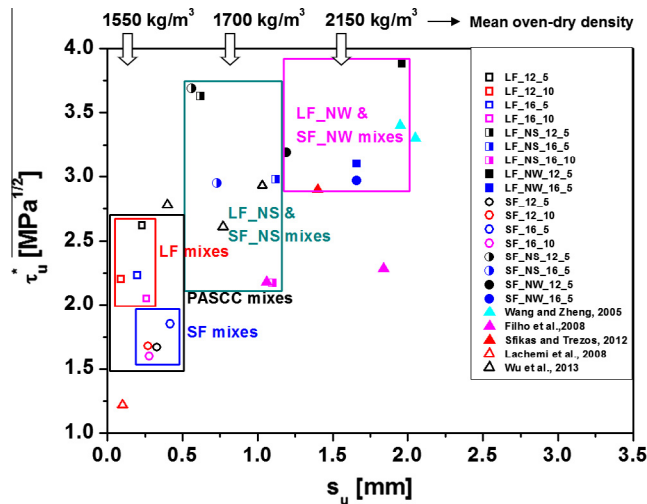


Fig. 10. Normalized bond stress versus ultimate slip for all direct pull-out tests specimen groups.

Table 6

Values for β and ν for each configuration of beam-type specimens.

Beam type	L_s [mm]	d [mm]	β [–]	ν [–]
X_12_10	250	100	1.250	10
X_16_10	450	150	1.500	10
X_12_5	108	100	0.540	5
X_16_5	160	150	0.533	5

Values for β and ν for each configuration of beam-type specimens are given in Table 6.

Beam test results are given in Table 7 in terms of: (i) bond strength (τ_u), (ii) normalized bond strength (τ_u^*), (iii) ultimate slip (at the moment when splitting failure occurs, s_u), (iv) bond stress at slippage of 0.01 mm, 0.1 mm, 1.0 mm and their mean value ($\tau_{0.01}$, $\tau_{0.1}$, $\tau_{1.0}$ and τ_m , respectively) and (v) failure mode (pull-out or steel yielding).

Tabulated values for each specimen group correspond to mean values calculated from two identical specimens and to the standard deviations thereof. Steel yielding failure occurred only in two cases, namely in specimens SF_16_10 and SF_NW_16_10 (one specimen of each group). The aforementioned specimens' results are not taken into account in Table 7. Representative bond stress – slip curves are given in Fig. 11 for all specimen groups.

Optical observation of the specimens verified that due to the self-compacting characteristics of the PASCC and NWSCC mixes the steel moulds were adequately filled producing smooth and defect-free concrete surfaces. Moreover, despite the

mixtures' flowability, no cement paste penetrated into the unbonded length of the rebars. All beam specimens (with two exceptions) failed due to rebar pull-out. However, this failure was not accompanied by cracks along the rebars.

In agreement with previous studies (focusing on the steel-to-NWSCC bond behavior, see [23,27]) beam test results indicate that contradictory to the case of direct pull-out tests maximum normalized bond stress τ_u^* increases for increasing rebar diameter (Fig. 12). This trend (valid for rebar diameters up to 16 mm) can be related to the following conditions. During bending (and for the same total force applied to the beam) larger tensile stresses are developed along the small diameter rebars in comparison to those developed along large diameter ones (bond stresses being proportional to tensile ones). In addition, it is probable that the detrimental effect of air and bleeding water entrapment beneath rebars during casting to bond conditions is more intense for rebars with small diameters than for rebars with large ones.

The aforementioned increase in τ_u^* was larger for lower mix densities (PASCC) and for shorter bond lengths. Mix SF_16_5 exhibited a 30% increase in τ_u^* compared to SF_12_5 while the respective increase for SF_NW_16_10 amounted to 6%.

As in the case of direct pull-out tests and for the same reasons, the increase of bond length led to decreasing of the maximum normalized bond stress, as shown in Figs. 12 and 13 (Fig. 13 also showing results from de Almeida Filho et al. [23] and Desnerck et al. [24] based on NWSCC). Specimens cast with mixes with SF addition (LF and SF blends) showed larger losses of bond capacity due to bond length increase when compared to counterpart specimens cast with mixes comprising LF as the single addition; this is attributed to the higher air content introduced in SF mixes leading to the entrapment of air bubbles along the rebar surface and, consequently, to the deterioration of the bond strength. τ_u^* reduction was approximately 15% for LF mixes and 25% for SF ones.

The substitution of pumice aggregates and pumice sand by normal-weight ones led invariably to a moderate increase of τ_u^* in the order of 10%.

When compared to direct pull-out tests (different failure modes taken aside), beam tests result in the development of lower τ_u^* values for PASCC specimens comprising limestone filler and for all NWSCC specimens (Fig. 14); the decrease amounts to approximately 10%, 20% and 40% for specimens cast with all-lightweight LF mixes and normal-weight SF and LF mixes, respectively. This outcome is in line with findings of previous works on normal-weight self-compacting or conventional concrete. For example, the same was observed for: (1) 50% of the SCC beam-type specimens compared to counterpart direct pull-out ones in the work of de Almeida Filho et al. [23] (pull-out cylinders with a bonded length of 50 and beams with a bonded length of 100 invariably failing in splitting and steel yielding, respectively); and (2) for all of the Wildermuth and Hofmann [39] specimens cast with conventional concrete (up to 100% higher bond strengths were obtained with pull-out cubes with a bonded length of 50 compared to beams with a bonded length of 100). The following possible reasons are theorized for this phenomenon:

- (1) In beam-type specimens the casting position (normal to the rebar under testing) is associated to unfavorable steel-to-concrete bond conditions (due to the formation of air and/or water pockets beneath the rebar); casting direction in direct pull-out specimens is usually parallel to the rebar under testing.
- (2) The test set-up of the direct pull-out test introduces compressive stresses in the region of the bonded length augmenting the transferrable bond strength.

Table 7

Beam test results.

Specimens	Bond strength	Normalized bond strength	Ultimate slip					Failure mode P/Y ^a
	τ_u [MPa] (St. dev.)	τ_u^* [MPa] ^{1/2} (St. dev.)	s_u [mm] (St. dev.)	$\tau_{0.01}$ [MPa] (St. dev.)	$\tau_{0.1}$ [MPa] (St. dev.)	$\tau_{1.0}$ [MPa] (St. dev.)	τ_m [MPa] (St. dev.)	
LF_12_5	12.73 (0.43)	2.07 (0.07)	1.72 (0.36)	4.62 (0.06)	9.30 (0.25)	12.23 (0.52)	8.71 (0.26)	P
LF_12_10	12.30 (0.05)	2.01 (0.07)	0.26 (0.02)	5.20 (0.28)	11.32 (0.06)	12.05 (0.13)	9.53 (0.07)	P
LF_16_5	14.88 (0.62)	2.44 (0.18)	2.01 (0.19)	4.65 (0.48)	10.92 (0.25)	14.41 (0.34)	9.99 (0.36)	P
LF_16_10	12.63 (0.38)	2.01 (0.02)	0.46 (0.17)	4.95 (0.52)	10.82 (0.04)	12.31 (0.16)	9.36 (0.24)	P
LF_NW_12_5	16.31 (0.73)	2.37 (0.07)	2.04 (0.38)	4.16 (0.75)	9.44 (0.02)	16.43 (1.74)	10.01 (0.31)	P
LF_NW_16_5	16.96 (0.54)	2.60 (0.08)	2.57 (0.15)	2.78 (0.86)	9.61 (0.85)	15.19 (0.45)	9.19 (0.17)	P
LF_NW_16_10	13.06 (0.38)	1.90 (0.02)	2.50 (0.03)	3.20 (0.01)	7.65 (0.71)	11.50 (0.04)	7.45 (0.22)	P
SF_12_5	13.34 (2.15)	2.19 (0.31)	2.01 (0.01)	3.75 (0.75)	10.02 (0.26)	12.79 (1.96)	8.85 (0.32)	P
SF_12_10	11.22 (0.18)	1.94 (0.11)	0.28 (0.08)	4.77 (0.63)	9.62 (0.15)	10.99 (0.02)	8.46 (0.27)	P
SF_16_5	14.36 (1.45)	2.53 (0.15)	1.59 (1.74)	5.20 (0.72)	11.19 (1.98)	13.55 (1.54)	9.98 (1.56)	P
SF_16_10	12.93 (–) ^b	2.12 (–)	0.22 (–)	2.69 (–)	5.89 (–)	9.21 (–)	5.93 (–)	1P/1Y
SF_NW_12_5	15.57 (0.08)	2.30 (0.04)	1.78 (0.14)	4.51 (2.55)	10.71 (2.14)	15.24 (0.23)	10.15 (1.64)	P
SF_NW_16_5	18.54 (0.58)	2.72 (0.08)	2.45 (0.13)	4.74 (1.69)	12.48 (0.33)	7.34 (0.52)	11.52 (0.32)	P
SF_NW_16_10	13.16 (–) ^b	1.97 (–)	2.43 (–)	2.62 (–)	4.45 (–)	6.91 (–)	4.66 (–)	1P/1Y

^a P for pull-out failure, Y for steel yielding.

^b One out of two specimens failed due to steel yielding (tabulated values correspond to the specimen exhibiting pull-out failure) – no standard deviation can be derived.

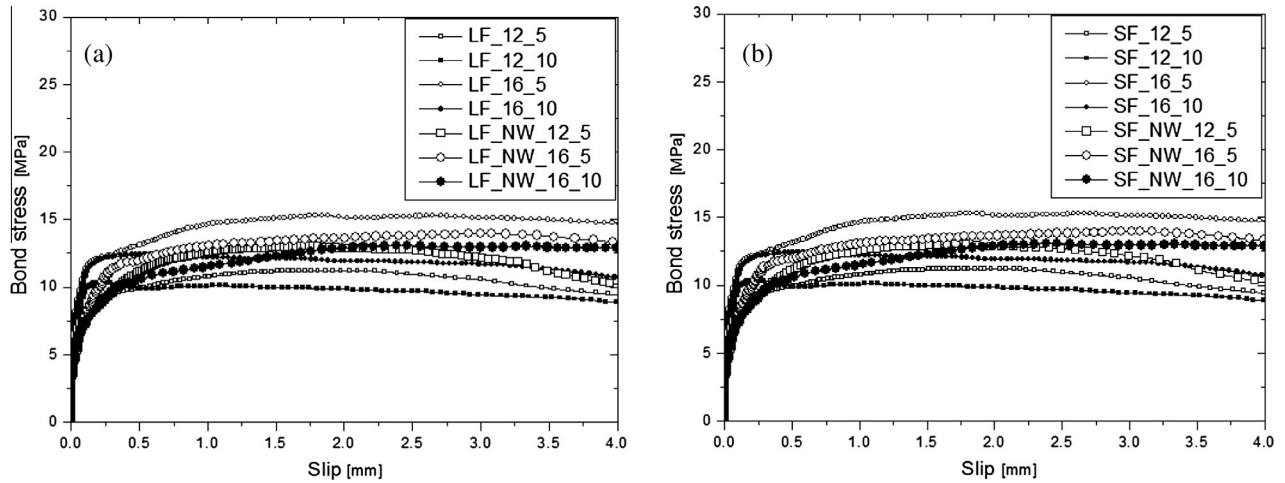


Fig. 11. Representative bond stress – slip curves for beam-type specimens: (a) LF_Y_Z and (b) SF_Y_Z.

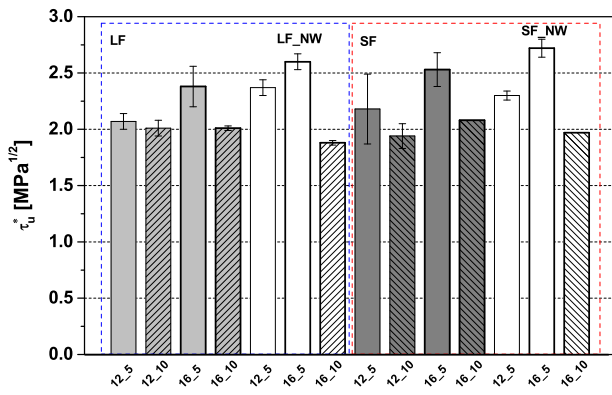


Fig. 12. Maximum normalized bond stress for beam tests.

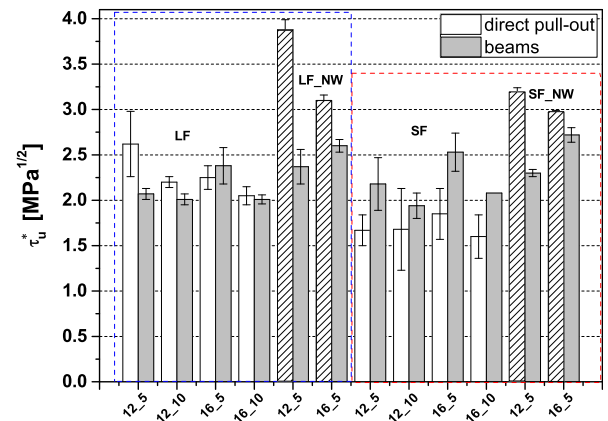


Fig. 14. Comparison of maximum normalized bond stress values derived from direct pull-out and beam type tests.

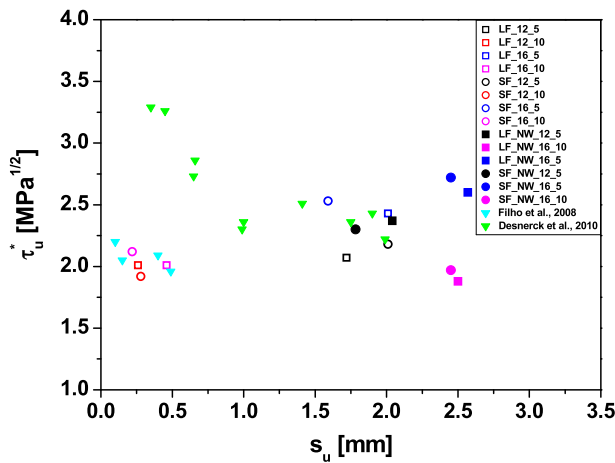


Fig. 13. Normalized bond stress versus slippage for all beam type specimen groups.

- (3) The assumption of uniform shear stress distribution along the rebar under testing is more valid for direct pull-out tests than for beam tests in which a more complex steel stress state develops due to the specimen's kinematics. Local shear stress concentrations may lead to premature deterioration of the steel–concrete interface.

Although it seems that confinement conditions were favorable in the case of specimens cast with all-lightweight SF mixes, the higher variations of τ_u^* values within the same SF_Y_Z specimen group challenges the validity of this observation.

2.5. Comparison to predicting equations proposed by the literature

Many authors have proposed relationships for the calculation of the peak bond resistance of steel rebar-to-concrete interfaces. Empirical expressions derived from regression analysis of experimental data focus mainly on the following parameters: i) mean concrete compressive strength f_c , ii) concrete cover c , iii) rebar diameter ϕ_s , and iv) bond length l_b . In this study the expressions used to compare both the confined (beam) and the unconfined (pull-out) test results are those of:

- Orangun et al. [40] [Eq. (4)]. This formulation was derived from – already available in the literature – beam specimens furnished with lap splices and cast with vibrated normal-weight concrete (VC); [Eq. (4)] was based on test results of beams lacking transverse reinforcement (i.e. unconfined lap splices). The companion formulation proposed by Orangun et al. [40] accounting for the presence of transverse reinforcement was not considered for comparison of the confined (beam) test results produced in this work as transverse reinforcement in the herewith presented beam-type specimens was not in contact with the bar undergoing pull-out (in contrast to the specimens comprising the database of Orangun and coworkers). It is noted that specimens failing due to splitting after steel yielding were disregarded from the data fitting process conducted by the aforementioned authors.
- Chapman and Shah [41], [Eq. (5)]. The formulation was derived from own direct (unconfined) pull-out VC specimens without differentiating between splitting, pull-out or steel yielding failure modes.
- Al-Jahdali et al. [42] [Eq. (6)]. The formulation was derived from own direct pull-out high-strength VC specimens without differentiating between failure modes such as splitting, pull-out, tensile concrete fracture or steel rupture.
- Aslani and Nejati [43], [Eq. (7)]. The formulation was derived from a compilation of – already available in the literature – direct pull-out and beam-type NWSCC specimens without differentiating between dissimilar failure modes.
- Model Code 2010 (MC2010 – [44]) [Eq. (8)]. Eqs. (8a) and (8b) are proposed by MC2010 for splitting and pull-out failure, respectively. It should be noted that Eq. (8a) is derived from the semi-empirical equation provided in MC2010 for

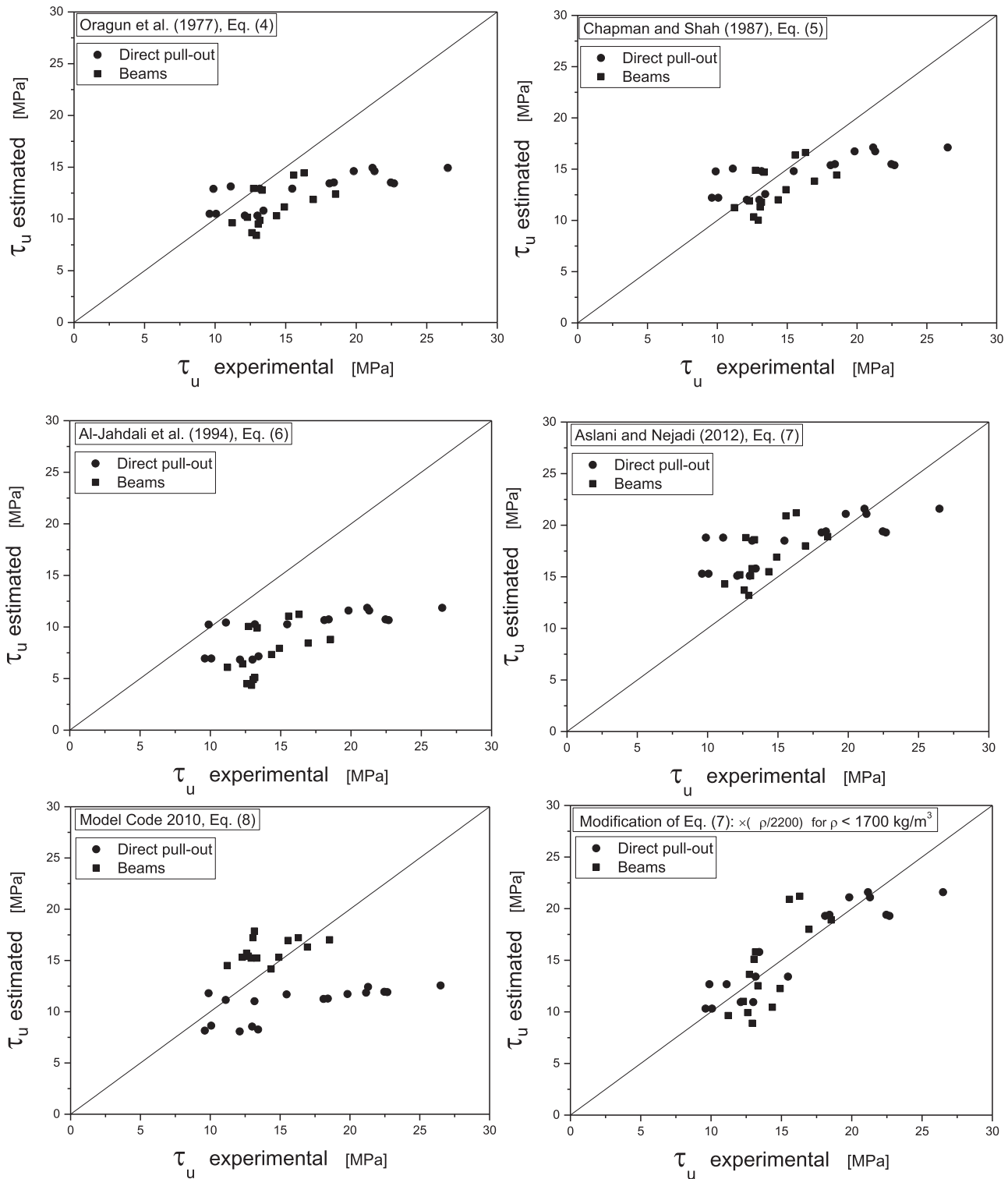


Fig. 15. Estimated (theoretical) versus experimental ultimate bond stress values. Empirical formulations provided by of: (a) Orangun et al. [40], (b) Chapman and Shah [41], (c) Al Jahdali et al. [42], (d) Aslani and Nejadi [43], (e) Model Code 2010 [44] and (f) this work (modification of Eq. (7)).

the calculation of the mean reinforcement stress in the case of unconfined ribbed bars and “good” casting position (note: here bars were placed at a 90° inclination to the horizontal during concreting). The aforementioned equation was used despite the fact that it is valid for $0.5 < \frac{c}{\phi_s} < 3.5$ (in this work $\frac{c}{\phi_s} = 4.5$ for pull-out specimens which predominantly failed due to splitting). Eq. (8b) also assumes “good” bond conditions. Eqs. (8a) and (8b) were used to predict direct pull-out and beam test results, respectively, as the former and the latter failed almost invariably due to splitting and pull-out, respectively.

The only formulation found in the literature that is specifically developed for lightweight SCC is that of Bae [45] (Eq. (9)); nevertheless, it is not considered for comparison in this work as it does not account for the $\left(\frac{\phi_s}{b}\right)$ parameter.

$$\tau_u = \left\{ 1.22 + 3.23 * \frac{c}{\phi_s} + 53 * \frac{\phi_s}{l_b} \right\} * \sqrt{f_c} \quad [\text{psi}] \quad (4)$$

$$\tau_u = \left\{ 3.5 + 3.4 * \frac{c}{\phi_s} + 57 * \frac{\phi_s}{l_b} \right\} * \sqrt{f_c} \quad [\text{psi}] \quad (5)$$

$$\tau_u = \left\{ -0.879 + 0.324 * \frac{c}{\phi_s} + 5.79 * \frac{\phi_s}{l_b} \right\} * \sqrt{f_c} \quad [\text{MPa}] \quad (6)$$

$$\tau_u = \left\{ 0.672 \left(\frac{c}{\phi_s} \right)^{0.6} + 4.8 * \frac{\phi_s}{l_b} \right\} * (f_c)^{0.55} \quad [\text{MPa}] \quad (7)$$

$$\tau_u = \tau_{bu,split} = 13.5 \left(\frac{25}{\phi_s} \right)^{0.25} \left(\frac{f_c}{25} \right)^{0.25} \left(\frac{c}{\phi_s} \right)^{0.25} \left(\frac{\phi_s}{l_b} \right)^{0.45} \quad [\text{MPa}] \quad (8a)$$

$$\tau_u = \tau_{b,max} = 2.5 \sqrt{f_c} \quad [\text{MPa}] \quad (8b)$$

$$\tau_u = 0.85 \left(\frac{c}{\phi_s} \right)^{0.17} * (f_c)^{0.58} \quad [\text{MPa}] \quad (9)$$

It is useful to note that the mean concrete compressive strength in Eqs. (4)–(6) has been estimated from compressive tests on cylindrical specimens [e.g. 76 mm × 152 mm for Chapman and Shah [41], unspecified for the others], whereas the mean concrete compressive strength of all fitted data from Aslani and Nejadi [43] has been converted to the one corresponding to 100 mm × 200 mm cylinders. Papanicolaou and Kaffetzakis [14] report that the ratio of 150 mm × 300 mm cylinder compressive strength to that derived from 150 mm cubic specimens for PASC is equal to 0.9. This means that, generally, the minimum ratio of cylinder compressive strength (cylinder being of any acceptable size) to that derived from 150 mm cubic specimens for PASC is equal to 0.9. Additionally, the RILEM report on mechanical properties of SCC – see Chapter 2 by Desnerck et al. [46] – quotes several studies to prove that a 150 mm × 300 mm cylinder to 150 mm cube conversion factor for NWSCC of 0.9 is advisable. Hence, if the concrete compressive strengths for all mixes produced in this work remain uncorrected (i.e. not converted to equivalent cylinder compressive strengths) τ_u is overestimated by only 5%–6% at most. Therefore, Eqs. (4)–(8) were applied in order to compute the theoretical τ_u values using the mean 150 mm cube compressive strengths given in Table 2.

Estimated (theoretical) versus experimental ultimate bond stress (peak bond resistance) values are illustrated in Fig. 15 for both direct pull-out and beam specimens through parity plots. Results indicate that (if both direct pull-out and beam data sets are considered) linear correlation between (estimated, experimental) pairs of τ_u values is rather poor with R-squared values being equal to 0.439, 0.451, 0.377 and 0.475 for Eqs. (4)–(7), respectively and slope values ranging between 0.31 [for Eq. (4)] and 0.42 [for Eq. (7)]. No correlation is achieved for Eqs. (8a) and (8b). In rough terms, the majority of direct pull-out test data is underestimated by all formulations (by 17%–40%) except that of Aslani and Nejadi [43] which provides a mean overestimation of approximately 30%. The same applies for the majority of beam test data (the underestimation varying between 15% and 47%) with the exception being extended to the MC2010 prediction that overestimates τ_u by 20% [similar to Eq. (7)].

From the above considerations it becomes clear that the most promising of predicting formulations for τ_u is that of Aslani and Nejadi [43]. Also, from Fig. 15(d) it is seen that the deviations from the 'y = x' line are maximized for the all-lightweight group of specimens ($\rho < 1700 \text{ kg/m}^3$). In an attempt to modify the best performing formulation and conforming to the density-related observation described in previous sections (relating to bond strength) it is proposed to reduce the computed values of τ_u for PASC mixes with an oven-dry density less than 1700 kg/m^3 by multiplying Eq. (7) with the factor $(\frac{\rho}{2200})$. Indeed, by doing so both the R-squared value and the slope of the correlated data improve ($R^2 = 0.677$ and slope = 0.85, see Fig. 15(f)). It is evident that the size of experimental data presented herein does not allow for safe statistical treatments and that more pertinent test results are needed in order to verify the above-described modification.

3. Conclusions

This paper presents an experimental program aiming at the investigation of bond characteristics of deformed steel rebars embedded in pumice aggregate self-compacting concrete. Steel-to-concrete bond was studied under both unconfined and confined conditions through direct pull-out and beam-type specimens, respectively. The effect of partial and full replacement of lightweight aggregates by normal-weight ones received special attention. According to the results of this work, the following main conclusions are drawn:

- Increase of bond length leads to decreasing of the maximum normalized bond stress for both types of tests (direct pull-out and beam).

- Contradictory to the case of direct pull-out tests, maximum normalized bond stress τ_u^* increases for increasing rebar diameter the magnitude of this increase being dependent upon both the bond length and the oven-dry density of the mix (larger for lower mix densities and for shorter bond lengths). A plausible explanation of this phenomenon is given in the paper.
- For the case of direct pull-out tests (resulting in splitting failure modes), the maximum normalized bond stress and the ultimate slip increase with increasing concrete density being the result of partial or full replacement of lightweight aggregates with normal-weight ones. This increase is significant (more than 40%) for oven-dry densities in the range of 1550 kg/m^3 – 1700 kg/m^3 . Strength gains for densities close to or higher than the upper oven-dry density limit for lightweight concrete (2000 kg/m^3) are limited. Moderate bond strength gains due to concrete density increase are also noted for the case of beam tests (resulting in pull-out failure modes). More specifically, if rebar pull-out takes place the all-lightweight SCC bond strength is up to 30% lower than that of NWSCC.
- When compared to direct pull-out tests, beam tests result in the development of lower τ_u^* values for PASC specimens comprising limestone filler and for NWSCC specimens (Fig. 13); this decrease amounts to approximately 10%, 20% and 40% for specimens cast with all-lightweight LF mixes and normal-weight SF and LF mixes, respectively. On the contrary, confinement conditions were proved to be favorable in the case of specimens cast with all-lightweight SF mixes with an average of 30% increase in τ_u^* .
- The formulation that best fits the experimental data produced in this work is a modification of the expression proposed by Aslani and Nejadi [43]. A reduction factor equal to $(\rho/2200)$ is introduced for PASC mixes with an oven-dry density less than 1700 kg/m^3 .

References

- [1] T.A. Holm, *Durability of Structural Lightweight Concrete*, 126, ACI Special Publication, 1991.
- [2] C. Ozyildirim, *Durability of structural lightweight concrete*, 2008 Concrete Bridge Conference, 2008. St Louis, MO.
- [3] ACI Committee 213, *Guide for Structural Lightweight-Aggregate Concrete*, (ACI 213R-03) American Concrete Institute, Farmington Hills, MI, 2003, p. 38.
- [4] O. Sengul, S. Azizi, F. Karaosmanoglu, M.A. Tasdemir, Effect of expanded perlite on the mechanical properties and thermal conductivity of lightweight concrete, *Energy Build.* 43 (2) (2011) 671–676.
- [5] ACI 216.1, *Standard Method for Determining Fire Resistance of Concrete and Masonry Construction Assemblies*, ANSI/ACI216.1-97/TMS-0216-97, The Masonry Society, Boulder Co., 1997.
- [6] S. Chandra, L. Berntsson, *Lightweight Aggregate Concrete*, Elsevier, 2002.
- [7] S.H. Müller, M. Haist, *Self-compacting Lightweight Concrete*, BFT magazine, 2004. 12/2004.
- [8] M. Kaffetzakis, C. Papanicolaou, Bond behavior of pumice aggregate self-compacting concrete (PASC), *Bond in Concrete 2012 4th International Symposium*, 2012. Brescia, Italy.
- [9] C.L. Hwang, M.F. Hung, Durability design and performance of self-consolidating lightweight concrete, *Constr. Build. Mater.* 19 (2005) 619–626.
- [10] M. Hubertova, R. Hela, The effect of metakaolin and silica fume on the properties of lightweight self-consolidating concrete, *ACI Mater. J.* (2007).
- [11] M. Kaffetzakis, C. Papanicolaou, Durability aspects of pumice aggregate self-compacting concrete (PASC): comparison with normal-weight SCC (NWSCC), *Concrete Structures for Sustainable Community, fib Symposium*, 2012. Stockholm, Sweden.
- [12] T. Uygunoğlu, I.B. Topçu, Thermal expansion of self-consolidating normal and lightweight concrete at elevated temperature, *Constr. Build. Mater.* 23 (2009) 3063–3069.
- [13] C. Papanicolaou, M. Kaffetzakis, Pumice aggregate self-compacting concrete, 16th National Conference on Concrete (2009). Cyprus, Paphos.
- [14] C. Papanicolaou, M. Kaffetzakis, Lightweight aggregate self-compacting concrete: state-of-the-art & pumice application, *Advanced Concrete Technology* 9 (1) (2011) 15–29.
- [15] P. Gambarova, Bond in reinforced concrete: Where do we stand today?, *Bond in Concrete 2012 4th International Symposium*, 2012 Brescia, Italy.

- [16] K. Lundgren, Three dimensional modelling of bond in reinforced concrete: theoretical model, experiments and applications (PhD dissertation), Chalmers University of Technology, Sweden, 1999.
- [17] K.M.A. Hossain, Bond characteristics of plain and deformed bars in lightweight pumice concrete, *Constr. Build. Mater.* 22 (2008) 1491–1499.
- [18] M. Lachemi, S. Bae, K.M.A. Hossain, M. Shamaran, Steel-concrete bond strength of lightweight self-consolidating concrete, *Mater. Struct.* 42 (2009) 1015–1023.
- [19] O. Karahan, K.M. Hossain, E. Ozbay, M. Lachemi, E. Sancak, Effect of metakaolin content on the properties self-consolidating lightweight concrete, *Constr. Build. Mater.* 31 (2012) 320–325.
- [20] Z. Wu, Y. Zhang, J. Zheng, Y. Ding, An experimental study on the workability of self-compacting lightweight concrete, *Constr. Build. Mater.* 23 (2009) 2087–2092.
- [21] W. Zhu, M. Sonebi, P.J.M. Bartos, Bond and interfacial properties of reinforcement in self-compacting concrete, *Mater. Struct.* 37 (2004) 442–448.
- [22] M.R. Esfahani, M. Lachemi, M.R. Kianoush, Top-bar effect of steel bars in self-compacting concrete (SCC), *Cem. Concr. Compos.* 30 (2008) 52–60.
- [23] F.M. De Almeida Filho, M.K. El Debs, A.L.H.C. El Debs, Bond-slip behavior of self-compacting concrete and vibrated concrete using pull-out and beam tests, *Mater. Struct.* 41 (6) (2008) 1073–1089.
- [24] P. Desnerck, G. De Schutter, L. Taerwe, Bond behaviour of reinforcing bars in self-compacting concrete: experimental determination by using beam tests, *Mater. Struct.* 43 (2010) 53–62.
- [25] V. Boel, P. Helinckx, P. Desnerck, G. De Schutter, Bond behaviour and shear capacity of self-compacting concrete, in: K.H. Khayat, D. Feys (Eds.), *Design, Production and Placement of Self-Consolidating Concrete*, RILEM Bookseries 1, 2010, pp. 343–353, http://dx.doi.org/10.1007/978-90-481-9664-7_29, RILEM 2010.
- [26] L.N. Thrane, C. Pade, C. Idzerda, M. Kaasgaard, Effect of rheology of SCC on bond strength of ribbed reinforcement bars, in: K.H. Khayat, D. Feys (Eds.), *Design, Production and Placement of Self-Consolidating Concrete*, RILEM Bookseries 1, 2010, pp. 367–377, http://dx.doi.org/10.1007/978-90-481-9664-7_29, RILEM 2010.
- [27] S. Cattaneo, G.P. Rosati, Bond between steel and self-compacting concrete: experiments and modelling, *ACI Struct. J.* 106 (4) (2009) 540–550.
- [28] K.H. Khayat, P. Desnerck, Chapter 4 – Bond properties of self-compacting concrete, in: K.H. Khayat, G. De Schutter (Eds.), *Mechanical Properties of Self-Compacting Concrete*, RILEM State-of-the-Art Reports 14, Springer International Publishing, 2014, pp. 95–139.
- [29] CUR Report No. 173, *Structural Behaviour of Concrete with Coarse Lightweight Aggregates*, 1994.
- [30] E. Sancak, O. Simcek, A.C. Apay, A comparative study on the bond performance between rebar and structural lightweight pumice concrete with/without admixture, *Int. J. Phys. Sci.* 6 (14) (2011) 3437–3454.
- [31] M. Kaffetzakis, C. Papanicolaou, Mix proportioning method for lightweight aggregate SCC (LWASCC) based on the optimum packing point concept, in: M. Fardis (Ed.), *Innovative Materials and Techniques in Concrete Construction*, ACES Workshop, Springer, 2012, ISBN 978-94-007-1996-5.
- [32] EN 206, *Concrete – Specification, Performance, Production and Conformity*, 2013.
- [33] Rilem-FIP-CEB, Bond test for reinforcing steel: 1-beam test (7-II-28 D). 2-Pullout test (7-II-128): tentative recommendations, *Mater. Struct.* 6 (32) (1973) 96–105.
- [34] EN 10080, *Steel for the Reinforcement of Concrete, Weldable, Ribbed Reinforcing Steel*, 2006.
- [35] L.N. Lowes, Finite element modeling of reinforced concrete beam-column bridge connections (Doctoral dissertation), University of California, Berkeley, 1999.
- [36] L.A. Lutz, P. Gergely, Mechanics of bond and slip of deformed bars in concrete, *J. Proc.* 64 (11) (1967) 711–721.
- [37] G. Wang, J. Zheng, Bond behaviors of self compacting concrete, SCC 2005 China: 1st International Symposium on Design, Performance and Use of Self Consolidating Concrete, RILEM Publications SARL, 2005.
- [38] K. Trezos, I. Sfikas, C.G. Papios, Influence of water-to-binder ratio on top-bar effect and bond variation across length in self-compacting concrete specimens, *Cem. Concr. Compos.* 48 (2014) 127–139, 04/2014.
- [39] A. Wildermuth, J. Hofmann, Effect of the bond behaviour of rebars and its evaluation by simplified test specimens, *Bond in Concrete 2012*, International Symposium, 2012, Brescia, Italy.
- [40] C.O. Orangun, J.O. Jirsa, J.E. Breen, A reevaluation of test data on development length and splices, *ACI J.* 74 (3) (1977) 114–122.
- [41] R.A. Chapman, S.P. Shah, Early-age bond strength in reinforced concrete, *ACI Mater. J.* 84 (6) (1987) 501–510.
- [42] F.A. Al-Jahdali, F.F. Wafa, S.A. Shihata, Development Length for Straight Deformed Bars in High-strength Concrete, 149, *ACI Special Publication (SP-149)*, 1994, pp. 507–522.
- [43] F. Aslani, S. Nejadi, Bond behavior of reinforcement in conventional and self-compacting concrete, *Adv. Struct. Eng.* 15 (12) (2012) 2033.
- [44] Model Code 2010-Final Draft, *Fédération Internationale du Béton fib/International Federation for Structural Concrete*, 2010.
- [45] S. Bae, Mix design, formwork pressure and bond characteristics of special self-consolidating concrete (Master Thesis), Ryerson University, Toronto, Canada, 2006.
- [46] P. Desnerck, V. Boel, B. Craeye, P. Van Itterbeeck, Chapter 2 – mechanical properties, in: K.H. Khayat, G. De Schutter (Eds.), *Mechanical Properties of Self-Compacting Concrete*, RILEM State-of-the-Art Reports 14, Springer International Publishing, 2014, pp. 15–71.